IEEE Access
Multidisciplinary ⋮ Rapid Review ⋮ Open Access Journal

Received 5 July 2023, accepted 30 July 2023, date of publication 3 August 2023, date of current version 24 August 2023.

Digital Object Identifier 10.1109/ACCESS.2023.3301612

RESEARCH ARTICLE

Fault Current Improved Grey Slope Relational Analysis Based Unit Protection Scheme for DC Distribution Lines

ENSHU JIN, XIAOCHEN HU, XINGRU WU, AND SHUANGSHUANG ZHANG
School of Electrical Engineering, Northeast Electric Power University, Jilin 132011, China

Corresponding author: Xiaochen Hu (h1035295150@foxmail.com)

This work was supported by the National Key Research and Development Program Smart Grid Technology and Equipment Key Special Project 2016YFB0900600.

ABSTRACT Multi-terminal flexible DC distribution line faults develop rapidly, and power electronic equipment has a poor ability to withstand overcurrent. To solve the aforementioned problem, a DC line unit protection scheme based on improved Grey Slope Relational Analysis (GSRA) of fault currents is proposed to address the issue of achieving a balance between the reliability and speed of relay protection for DC distribution lines. This scheme uses the fault current measured at both ends of the line under various operating conditions, and calculates the correlation between the current at both ends of the positive and negative lines using the slope distance and polarity of the current increments. Based on this, GSRA is used to analyze the correlation of fault signals so that line faults can be eliminated quickly. This protection scheme allows the selectivity of traditional unit protection to be improved. Simulations using PSCAD/EMTDC have shown that this method can achieve fault discrimination and fault pole selection by simultaneously measuring the current at both ends of the line. This fast protection action is not affected by the line distribution capacitance and converter blocking, strong resistance to transition resistance and noise interference, and reliable identification under heavy loads and high-resistance ground faults.

INDEX TERMS DC distribution system, current increment, slope relational analysis, unit protection, fault detection.

NOMENCLATURE AND ABBREVIATIONS

GSRA	grey slope relational analysis.
MTDC	multi-terminal dc.
CLR	current limiting reactor.
MMC	modular multilevel converter.
VSC	voltage source converter.
DAB	dual active bridge.
DCT	dc transformer.
ISOP	input series output parallel.
R_f	transition resistance.
H	the head of the line.
E	the end of the line.
P	positive line.
N	negative line.
I_{Xy}	measured current at the y-pole of the X-end of the line.
PPG	positive pole-to-ground.
NPG	negative pole-to-ground.
PP	pole-to-pole.
ΔI	current increment sequence.
σ	the slope distance of positive and negative pole lines.
r	the slope correlation sequence.
γ	the slope relation.

The associate editor coordinating the review of this manuscript and approving it for publication was Feng Wu.

I. INTRODUCTION

In recent years, there has been an increasing demand for renewable energy worldwide, as the use of traditional fossil fuels has contributed to global warming, causing serious

environmental pollution [1], [2]. A flexible multi-terminal DC (MTDC) distribution system with low line losses, high transmission capacity, and efficient access to distributed energy sources has become the key to solving current power distribution problems and the development of power systems in the immediate future [3], [4]. However, the damping of the flexible DC distribution network is low, and the overcurrent generated by the fault may destroy the power electronics within milliseconds, and the traditional protection scheme with low speed is no longer applicable, which puts higher requirements on relay protection [5], [6]. In addition, line faults account for the vast majority of DC system faults, and the fast and reliable identification of faulty lines is a key and difficult point in the development of relay protection technology for DC distribution systems [7], [8].

At the present stage, the protection scheme for DC lines is mainly divided into two categories: non-unit protection and unit protection. Non-unit protection measures electrical quantities at the one end of the DC line without transferring the measured values to the other end of the line and determines faults directly based on the measured values at the single end, which has a high speed. In [9], a fast fault recognition scheme based on measured current was proposed, but this scheme could not withstand high-intensity noise. References [10] and [11] constructed protection schemes used the traveling wave of the initial current and the voltage drop of the initial current limiting reactor (CLR), respectively, and such methods require high sampling frequency. References [12] and [13] used the current fault component of the CLR and the voltage integral of the CLR to discriminate line faults and achieve fast fault isolation, respectively, such methods require additional measurement points and are limited by the current limiting effect of the CLR, which cannot withstand higher transition resistance. References [14] and [15] analyzed aspects such as line frequency parameter models, fault characteristics, and quantify the sensitivity of the flexible DC fault characteristics for different influencing factors, which have complicated threshold rectification of such protection schemes. In general, non-unit protection has the disadvantages of complex threshold rectification, reliance on simulation, inability to tolerate high transition resistance and noise interference, and large influence by system operation modes.

Unit protection treats the DC line as a unit, measures electrical quantities at both ends of the line, and compares the data at each end through the communication channel to decide whether to operate for protection, unit protection has a very high selectivity and the simpler threshold adjustment makes the reliability of unit protection relatively higher. There is a relatively large amount of literature on unit protection of DC lines. For example, in [16], the Bhattacharyya distance method was used to determine the fault location based on the conclusion that the measured current waveform characteristics were different on both sides of the line in the case of internal and external faults. In [17], the Pearson correlation coefficients were used to realize the recognition of faulty lines based on the difference in voltage waveforms on both sides of the line at different fault locations. In [18], the protection achieved fault recognition by calculating the transient voltage ratio of the CLR on both sides of the line. In [12], an Event-based protection scheme that requires fewer transmission data and higher speed was proposed. Protection schemes using the difference of fault components of line voltage and current under different location faults were proposed in [19] and [20], respectively, such methods have high communication requirements and poor interference immunity. The current differential protection proposed in [21] and [22] can recognize faults quickly and accurately, however, they are susceptible to interference by transition resistance and line-distributed capacitance. References [23] and [24] used traveling waves for fault recognition and pole selection, such methods require extremely high sampling frequency, and short DC distribution lines make the cost of sampling equipment increase significantly, whether traveling waves sampling equipment for transmission system are suitable for distribution system is still open to discussion. Unit protection has the problems of dependence on communication and lower speed, how to improve the speed as much as possible while ensuring the reliability and selectivity of unit protection has become the focus of research on unit protection.

In response to the above problems, this paper proposes a protection scheme based on an improved Grey Slope Relational Analysis (GSRA) of fault currents. First, we calculated the current increments on either side of the positive and negative DC lines. Then, the correlation of the currents at both ends of the positive and negative lines was calculated by extracting their slope distances and polarities. Finally, fault recognition and fault pole selection were realized using GSRA. The protection is lower for communication requirements, the principle is simple, it is unaffected by the transition resistance and loads current, and it has better tolerance to changes in system operation modes and disturbances such as noise. The protection scheme without initiation criteria is not affected by converter blocking and has higher speed and reliability. The feasibility of the protection scheme was verified by simulating and analyzing different working conditions using the PSCAD/EMTDC platform.

II. FLEXIBLE DC DISTRIBUTION SYSTEM TOPOLOGY

The topology of the multi-terminal ring flexible DC distribution system is illustrated in Fig. 1.

System primarily consists of AC systems, modular multilevel converter (MMC), voltage source converter (VSC), dual active bridge (DAB) DC converters, wind power systems, photovoltaic power systems, AC and DC loads, and DC distribution lines. The individual ports of the system are numbered as shown in the figure, where T1 and T2 are half-bridge submodules based on the MMC, which are connected to the AC system through a 110/10 kV transformer.

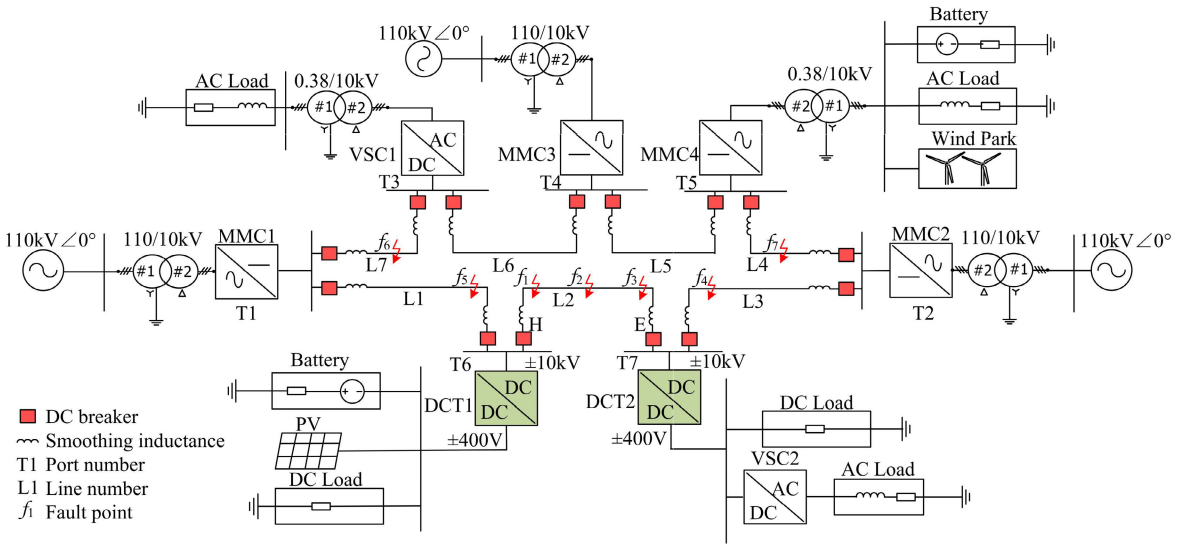

FIGURE 1. Multi-terminal flexible DC distribution system topology.

The system adopts a primary-secondary control strategy, with the true-bipolar MMC on port T1 as the master control station, using constant DC voltage and constant reactive power control. The true-bipolar MMC on port T2 is the slave control station using constant active and constant reactive power control. Port T3 is a three-phase, two-level VSC using constant AC-side voltage control, which connects the distribution network to the AC load. Pseudo-bipolar MMCs on ports T4 and T5 with islanding control and simultaneous access to AC loads and wind power systems. Ports T6 and T7 are DC transformers (DCT) that connect the distribution network to the DC load and PV system through a dual DAB cascade in the Input Series Output Parallel (ISOP) topology [25], [26]. DAB is controlled by single-phase shift control, which controls the low-voltage side voltage.

The ISOP-ISOP line is taken as the research object, and multiple fault points are set. Where $f1$ is set to 10% of the L2 line length, $f2$ is set to50 % of the L2 line length, $f3$ is set to 90% of the L2 line length, $f4$ is set to the beginning of the L3 line, and $f5$ is set to the end of the L1 line. When a fault occurs in the DC line of the system, the circuit breakers on both sides of the faulty line will isolate the fault in a timely manner, and the ring topology de-ringing for chain power, which ensures the reliability of the system power supply, a unit protection scheme based on improved GSRA of fault currents is proposed on this basis.

III. ANALYSIS OF FAULT CHARACTERISTICS OF DC DISTRIBUTION LINES

When a fault occurs on a DC distribution line, the DC voltage at the fault point drops significantly, and both sides of the line generate a fault current that flows simultaneously to the fault point. The fault current in the faulty initial stage mainly includes the discharge current of the large capacitor

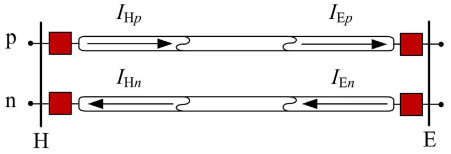

FIGURE 2. DC line current direction characteristics.

connected in parallel on the DC side of the VSC, DCT, and the MMC bridge arm. When the fault locations and types are different, the polarity and rising speed of the current measured at the measurement points at both ends of the line are also different. To meet the requirements of protection speed, this study takes line L2 as the object of study and analyses the fault information of the line current in the fault detection phase before converter blocking.

When the system is operating normally, make the positive direction of the current is the bus flow to the line. The equivalent network of the DC line is shown in Fig. 2.R_f is the transition resistance, side H is the head of the line, and side E is the end of the line; P for positive lines and N for negative lines; I_{Hp} and I_{Ep} are the positive line head measurement point current and positive line end measurement point current, respectively; I_{Hn} and I_{En} are the negative line head measurement point current and negative line end measurement point current, respectively. Meanwhile, the currents at the two ends of the positive line are in opposite directions, and the currents at the two ends of the negative line are also in opposite directions, confirming that the currents in the positive and negative lines are traversing currents.

A. ANALYSIS OF FAULT CURRENT POLARITY

When a single-pole grounded short-circuit fault occurs within the system (positive pole-to-ground (PPG) fault as an

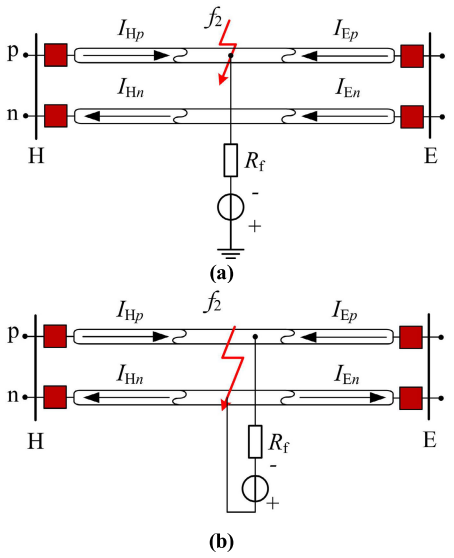

FIGURE 3. Directional characteristics of fault current in the DC line area: (a) PPG fault, (b) PP fault.

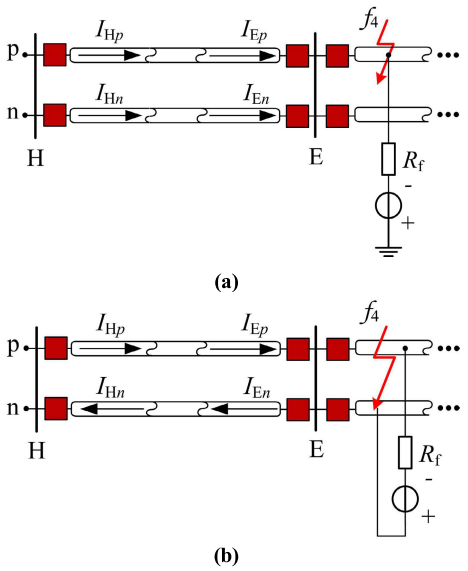

FIGURE 4. Directional characteristics of fault current outside the DC line area: (a) PPG fault, (b) PP fault.

example, a negative pole-to-ground (NPG) fault is similar to PPG), as shown in Fig. 3(a), the current at the fault pole flows simultaneously from both sides of the line to the fault point, and the head and end currents are positive and rapidly increasing, with the same polarity; the current of the healthy pole flows from the E side of the line to the H side of the line, and the currents at the head and the end are one positive and one negative with opposite polarity. When a PP short-circuit fault occurs within the system, as shown in Fig. 3(b), the current in the positive line flows simultaneously from both sides of the line to the fault point, and the currents at the head and the end are positive and of the same polarity. Negative line current flows from the fault point to both sides of the line, and the currents at the head and the end are negative and of the same polarity.

The equivalent network of the DC line when an external single-pole ground short-circuit fault occurs in the system is shown in Fig. 4(a). The fault pole and healthy pole currents flow from the head of the line to the end of the line and are traversing currents, the head and end currents show positive and negative currents, respectively, with opposite polarity. The equivalent network of the DC line when an external PP short-circuit fault occurs in the system is shown in Fig. 4(b). The currents at both ends of the positive line flow from the head of the line to the end of the line and are traversing currents, which have the opposite polarity of one positive and one negative. The currents at both ends of the negative line flow from the end of the line to the head of the line and are traversing currents, which have the opposite polarity of one negative and one positive.

The polarity characteristics of fault currents under different operating conditions are listed in Table 1. It is found that at least one pole of the line has the same current polarity at both ends when a fault occurs within the system; no current at either pole of the line has the same polarity when an external fault occurs in the system. On this basis, traditional longitudinal protection based on DC polarity has been proposed [20], with extremely rapid fault current change characteristics for fast fault discrimination; however, its reliability is relatively low, especially when affected by noise disturbance and load current.

TABLE 1. Polarity characteristics of fault currents under different operating conditions.

Operating conditions	Positive line		Negative line	
	H side	E side	H side	E side
Internal PPG fault	+	+	-	+
Internal NPG fault	+	-	+	+
Internal PP fault	+	+	-	-
Positive external fault	+	-	+/-	-/+
Reverse external fault	-	+	-/+	+/-

B. CHARACTERIZATION OF FAULT CURRENT INCREMENTS

Because a serious overcurrent phenomenon would occur after a DC system line fault, the information contained in the fault current also includes information besides the polarity such as the increment in the current. When a PG fault occurs in the DC line, the fault currents at both ends of the fault line grow rapidly in the same direction at approximately the same rate, and their increments are highly positively correlated, while the fault currents at both ends of the healthy line grow slowly at approximately the same rate, and their increments are negatively correlated. When a PP fault occurs in the DC line, the fault currents of both positive and negative lines grow rapidly in the same direction at approximately the same rate, and the current increments at both ends of

the positive and negative lines are highly positively correlated. When an external fault occurs in the DC line, the fault currents at both ends of either pole line grow at the same rate in reverse, and the current increments at both ends of the positive and negative pole lines are negatively correlated. To solve the problem of simultaneously taking into account the unit protection speed and reliability, this study calculates the GSRA of the fault current based on the increments and the slope of the fault current, combined with the polarity characteristics of the fault current. A unit protection scheme based on improved GSRA of fault currents is proposed.

IV. THE UNIT PROTECTION BASED ON CURRENT INCREMENTAL GSRA

A. GSRA

Grey Relational Analysis (GRA) is a dynamic series processing method that is widely used in many fields. Among them, GSRA can delve deeply into the data features of time-series curves, which are consistent with the characteristics of relay protection. Considering that the traditional GSRA method cannot respond to positive and negative correlations and has certain defects, this study improves on it to better adapt to the changing characteristics of fault current increments. The specific calculation steps of the improved GSRA are described in detail below [27].

To define the current increment sequence, the number of sampling points of each sequence defined in this paper needs to take into account the speed and reliability requirements of protection, positive and the negative lines on both sides of the fault current incremental expression are as follows (1).

$$\begin{cases} \Delta I_{xp_{(j,k)}} = I_{xp(j,k)} - I_{xp(j,k-1)} \\ \Delta I_{xn(j,k)} = I_{xn(j,k)} - I_{xn(j,k-1)} \end{cases} \tag{1}$$

In the above (1), j is the number of the incremental sequence, k is the number of different sampling points in each cycle, $k \in [2, N]$, N is the total number of sampling points in each cycle, and N is an integer, determined by the condition of the equipment sampled by the system. $\Delta I_{xp(j,k}$ and $\Delta I_{xn(j,k}$ are the increments of the positive and negative currents on the x side ($x = $ H, E represents the head and end of the line in turn) of the DC line, respectively.

The sequences of the positive and negative lines current increments are averaged, as shown in (2).

$$\begin{cases} \Delta \bar{I}_{xp_{(j)}} = \dfrac{1}{N-1}\left(\sum_{k=2}^{N} \left|\Delta I_{xp_{(j,k)}}\right|\right) \\ \Delta \bar{I}_{xn(j)} = \dfrac{1}{N-1}\left(\sum_{k=2}^{N} \left|\Delta I_{xn(j,k)}\right|\right) \end{cases} \tag{2}$$

In (2), $\Delta \bar{I}_{xp_{(j)}}$ and $\Delta \bar{I}_{xn(j)}$ are the mean values of x side increments of positive and negative pole lines.

The slope distance of the sequence of positive and negative current increments is calculated, as shown in (3).

$$\begin{cases} \sigma_{p(j,k)} = \dfrac{[\Delta I_{Hp(j,k)} - \Delta I_{Hp(j,1)}]}{\left|\Delta \bar{I}_{Hp_{(j)}}\right|} - \dfrac{[\Delta I_{Ep(j,k)} - \Delta I_{Ep(j,1)}]}{\left|\Delta \bar{I}_{Ep_{(j)}}\right|} \\ \sigma_{n(j,k)} = \dfrac{[\Delta I_{Hn(j,k)} - \Delta I_{Hn(j,1)}]}{\left|\Delta \bar{I}_{Hn(j)}\right|} - \dfrac{[\Delta I_{En(j,k)} - \Delta I_{En(j,1)}]}{\left|\Delta \bar{I}_{En(j)}\right|} \end{cases} \tag{3}$$

In (3), $\sigma_{p(j,k)}$ and $\sigma_{n(j,k)}$are the slope distance of positive and negative pole lines.

The slope correlation sequence $r_{y(j,k)}$ for the currents at both ends of the positive and negative lines is calculated, as shown in (4).

$$r_{y(j,k)} = \pm \frac{1}{1 + \left|\sigma_{y(j,k)}\right|} \tag{4}$$

In (4), y is either p or n, indicating positive and negative lines, respectively. To incorporate the polarity characteristics of the current into the algorithm, the sign is taken as positive when $\Delta I_{xp(j,k}$ and $\Delta I_{xn(j,k}$ have the same or opposite sign, and the sign is taken as positive when the product of the two is 0, otherwise, the sign takes the negative.

As a measure of the correlation of two time series by calculating the mean of the slope relation series, γ_y is the slope relation, as shown in (5).

$$\gamma_y = \frac{1}{N-1} \sum_{k=2}^{N} r_{y(j,k)} \tag{5}$$

This method improves the traditional GSRA by quantitatively analyzing the dynamic development process of the system while retaining the polarity characteristics of the time series to examine the degree of influence among the factors of the system or the contribution of the factors to the main behavior of the system. In terms of relay protection, this method preserves both the polarity characteristics of the post-fault currents and the characteristics of the growth rate and trend of the currents at both ends of different lines after the fault. If the two current series are perfectly positively correlated, then $\gamma_y = 1$, the opposite polarity and uncorrelated characteristics of the two current sequences reduce it. It can be seen that the slope relation can accurately identify the trend of the two curves and calculate the degree of correlation between them.

B. PROTECTION SCHEME DESIGN

The protection scheme described in this paper is derived from a combination of fault current GSRA and fault current polarity characteristics. This is reflected in the numerical calculation and symbolic parts in (4). The former can synthesize a set of average correlation data over a sampling period with higher protection reliability but a comparatively lower speed, and the latter can react to the fault characteristics for the first time when the current produces a sudden change after the fault, and the protection has higher speed, but the reliability

TABLE 2. Characteristics of slope relation under different operating conditions.

Operating conditions	Positive line	Negative line
Internal PPG fault	$\gamma_p > \gamma_{set}$	$\gamma_n < \gamma_{set}$
Internal NPG fault	$\gamma_p < \gamma_{set}$	$\gamma_n > \gamma_{set}$
Internal PP fault	$\gamma_p > \gamma_{set}$	$\gamma_n > \gamma_{set}$
External fault	$\gamma_p < \gamma_{set}$	$\gamma_n < \gamma_{set}$

is lower. The combination of the two can improve the speed and reliability of the fault-current GSRA, and the main part of the protection scheme is described below.

1) FAULT RECOGNITION

When the system operates normally or an external fault occurs, the current flowing through the positive and negative lines in the zone is the traversing current, with opposite polarity. The increments are one positive and one negative, and the calculated correlation has negative and small absolute values, so the protection would not be operated. When an internal fault occurs in the system, the current flowing through the fault pole is a non-traversing current with the same polarity and increments, and the calculated correlation is approximately 1, which is determined as an internal fault.

When the sign part of (4) is excluded, $\gamma_y = 1$ if the two time series are positively correlated and $\gamma_y = 0$ if the two time series are negatively correlated. When an internal fault occurs in the system, the currents at both ends of the fault pole line are positively correlated, and the calculated value of the slope correlation is approximated as 1. Regardless of the type of external fault in the system, the current at both ends of the same pole line is always negatively related, and the calculated value of the slope correlation is close to 0. The characteristics of slope correlation under different operating conditions are listed in Table 2. When an external fault occurs, γ_p and γ_n are both less than 1 and close to 0, this is used as the criterion for fault routing to escape the maximum γ_y setting rectification value γ_{set}.

2) FAULT POLE SELECTION

To improve the protection reliability, the fault pole selection scheme still adopts the GSRA characteristics of the fault current as the primary criterion and the fault current polarity as the secondary criterion for comprehensive development, and the fault pole selection scheme with improved slope correlation characteristics is discussed below.

Theoretically, the GSRA can be used to determine and select the fault line directly, but the above correlation is the calculated value of the ideal state. Mutual transformer measurement errors, noise, and other disturbances are simultaneously caused by the actual operation of the system at the same time. In addition, the instantaneous fault current reaches its peak within a few milliseconds after a fault occurs in the DC distribution system, which causes serious damage to the system. Combined with the requirements of the extensive literature on the protection time frame, the faulty line must be identified within 2ms [28].

TABLE 3. Parameters of the system.

Parameter	Value
Rated voltage at AC side /kV	110
Rated voltage at DC side /kV	± 10
DC line length /km	5
Number of DAB cascades	2
Support capacitance on input side /mF	2
Filter capacitance on output side /mF	2
Current limit inductor /mH	4

Combined with the definition of GSRA, when the system has a PPG fault, the calculated value of γ_p is approximately 1, whereas the single-pole ground fault will only cause a small disturbance to the healthy pole, and the change is not obvious within 1ms after the fault occurs. The direction of the fault current on both sides of the healthy pole line is negatively correlated, and the calculated value of γ_n is closer to 0. When a PP fault occurs in the system, the positive and negative fault currents rise rapidly within 1ms and are positively correlated, and the calculated values of γ_p and γ_n are about 1. Therefore, to ensure the reliability of the protection, the principle of γ_{set} is adjusted to evade the maximum value of γ_{out_max} in the case of an external fault, Considering the length and writing logic of the paper, the deduce process of γ_{set} is given in Appendix A. The expression of γ_{set} is shown in (6).

$$\gamma_{set} = K_{rel}\gamma_{out\_\max} \tag{6}$$

where γ_{set} is the adjustment threshold, which needs to consider a signal-to-noise ratio of 10 dB noise interference and $\pm 5\%$ of the measurement error of the transformer. K_{rel} is the reliability coefficient, which and takes values in the range (1.3,1.5).

The minimum value for internal faults under different operating conditions was divided by the adjustment threshold to calibrate the protection sensitivity coefficient [29].

$$K_{sen} = \gamma_{in\_\min}/\gamma_{set} \tag{7}$$

where K_{sen} is the sensitivity coefficient and takes values in the range of (1.25,1.35).

C. PROTECTION PROCESS

Considering the fault recognition criterion and fault pole selection criterion, the protection scheme shown in Fig. 5 is proposed.

V. SIMULATION VERIFICATION

Build a MTDC distribution system in PSCAD/EMTDC, as shown in Fig. 1. Line L2 is used as the protected line, and the measurement points are at the H and E ends of L2 line to verify the rationality of the protection scheme through simulation. The system parameters are listed in Table 3.

The polarity characteristics of the fault current and the GSRA would appear after the occurrence of the fault, which,

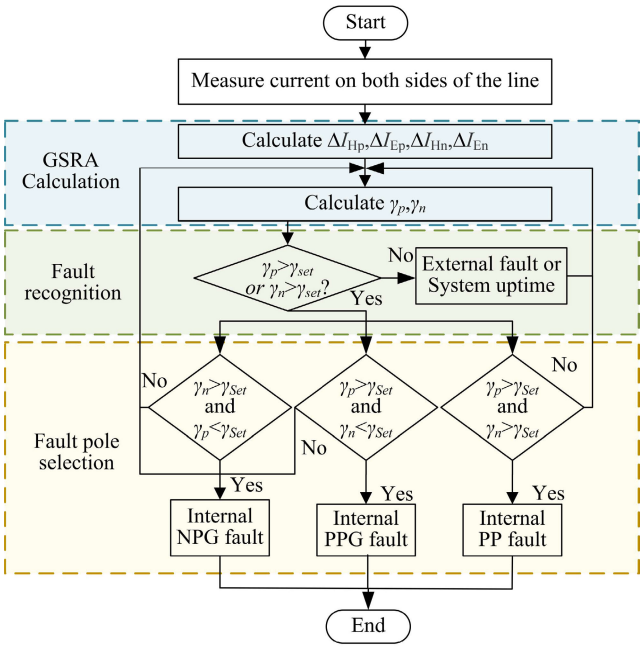

FIGURE 5. Flowchart of the protection scheme.

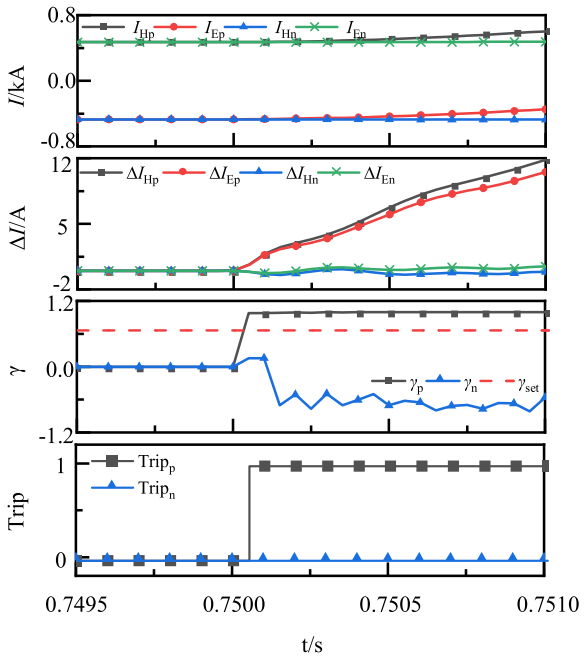

FIGURE 6. Simulation waveform of the internal PPG fault.

in combination with the protection scheme, could identify the fault. Theoretically, the higher the sampling frequency, the more sampling points there are at the same time, and the data will be relatively accurate. Considering the reliability and speed of protection, the selected simulation step is 50 us, and the sampling frequency is 20 kHz. The data window length of the real-time sampled current incremental sequence is 50 us, while the sampling window of the current incremental mean sequence is of the sliding time window type, which consists of three sampling points with a sliding time window length of 150 us.

According to the full-text analysis and simulation verification, γ_{set} evades the maximum value of the external fault for the adjustment principle, the final value is 0.7, and the introduction of the Trip signal indicates the correlation of the positive and negative lines on both sides of the current increments, defined as shown in (8).

$$\mathrm{Trip}_y = \begin{cases} 1, & \gamma_y \geqslant \gamma_{set} \\ 0, & \gamma_y < \gamma_{set} \end{cases} \tag{8}$$

The output value of Trip is used to determine whether the protection of each measurement point is operating, and when the signal sends 1 three times in a row, it is confirmed that a fault has occurred.

A. ANALYSIS OF PROTECTION BEHAVIOR

1) SIMULATION OF THE INTERNAL PPG FAULT

In this section, the internal PG fault will be verified, and a PPG fault occurs at $f2$ as an example, and the system runs until 0.75 s when a permanent fault occurs, and the simulation results are shown in Fig. 6. The figure shows the currents, current increments, current GSRA, and protection operations on the H and E sides of the line before and after the fault, respectively.

It can be found that when an internal single-pole ground fault occurs, the current polarity at both ends of the fault pole is positive, the current polarity at both ends of the healthy pole is one positive and one negative, the healthy pole current changes slowly, and the current polarity criterion speediness is reduced. Although the healthy pole current increments are almost zero in the initial stage of the fault, the fault pole current GSRA exceeds the adjusted value at the first sampling point immediately after the fault. The protection operates immediately when the Trip signal output at three consecutive sampling points is 1. This protection scheme can quickly and accurately identify an internal PPG fault.

2) SIMULATION OF THE INTERNAL PP FAULT

In this section, an internal PP metallic short-circuit fault is verified. A PP fault occurs at $f2$ as an example, and the system operates until 0.75 s when a permanent fault occurs, and the simulation results are shown in Fig. 7. It can be seen that the current polarity is the same on both sides of the positive line, and the current polarity is opposite on both ends of the negative line. Regardless of whether the line is positive or negative, the fault current increments at both ends of the line show a highly positive correlation trend, and at the first sampling point after the fault, both the positive and negative slope relations exceed the adjusted value. The protection operates immediately when the Trip signal output of three consecutive sampling points is 1. This protection scheme can quickly and accurately identify internal PP short-circuit faults.

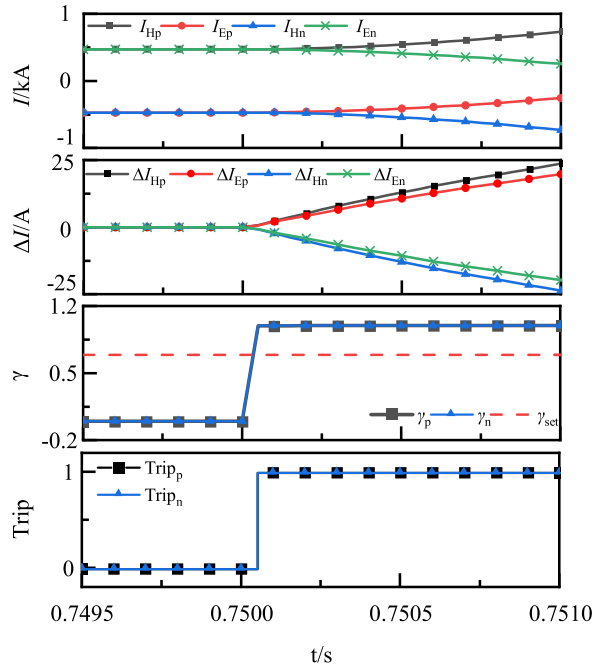

FIGURE 7. Simulation waveform of the internal PP fault.

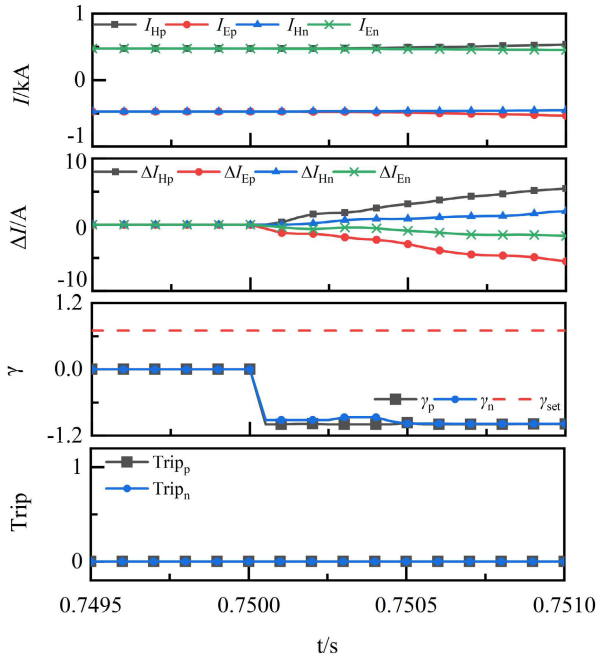

FIGURE 8. Simulation waveform of the external PPG fault.

3) SIMULATION OF THE EXTERNAL FAULT

In this section, an external fault will be verified. As an example, a PPG short-circuit fault occurs at $f4$, and the system runs to 0.75 s when a permanent fault occurs, and the simulation results are shown in Fig. 8. In terms of polarity, the currents on both sides of the positive and negative lines are traversing. In terms of the current GSRA, the fault current increments at both ends of the line show a negative correlation trend, the positive and negative slope relation of each sampling point after the fault does not exceed the adjusted value, the protection is not operated, and the protection scheme can accurately evade external faults.

B. ANALYSIS OF PROTECTION PERFORMANCE

1) THE INFLUENCE OF TRANSITION RESISTANCE

Because the fault current rise rate is weakened in the presence of transition resistance, the current correlation characteristics on both sides of the line will be reduced, and the traditional longitudinal protection, which depends on the change in current polarity, will have a rejection situation. The protection scheme proposed in this study integrates the characteristics of fault current polarity and GSRA, which can better tolerate the transition resistance. To verify that the protection scheme can withstand engineering short-circuit faults that may occur via transition resistance. Fig. 9 shows a PP fault via 20Ω transition resistor occurs at $f2$ as an example, and the system operates until 0.75 s when a permanent fault occurs.

The protection scheme can withstand the transition resistance that may occur in the real project. The maximum values of the first three improved GSRA and protection actions at each measurement point after the occurrence of the PPG fault

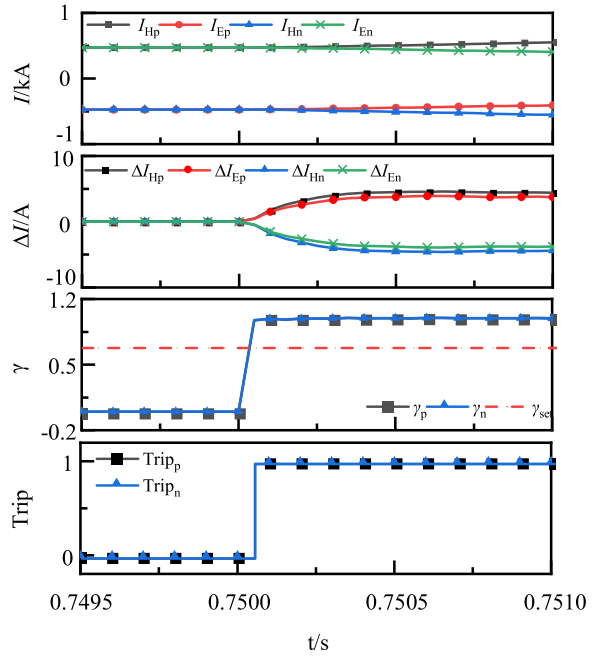

FIGURE 9. Internal PP fault via 20Ω transition resistor.

via transition resistance at different fault locations are listed in Table 4. Without considering the actual situation, algorithm can withstand a transition resistance of about 500Ω.

2) THE INFLUENCE OF THE LOAD CURRENT

When a high-resistance fault occurs in the system under a heavy load, the fault current variation is not evident, and the current polarity on both sides of the positive and negative

TABLE 4. Improved GSRA for short-circuit faults via transition resistance under different actual operating conditions.

Fault location	Transition resistance/Ω	GSRA		Discriminating results
		Positive line	Negative line	
	5	0.98	0.14	
$f1$	10	0.96	0.13	
	20	0.93	0.10	
	5	0.96	0.16	The internal fault
$f2$	10	0.98	0.20	
	20	0.98	0.09	
	5	0.98	0.18	
$f3$	10	0.95	0.19	
	20	0.94	0.12	

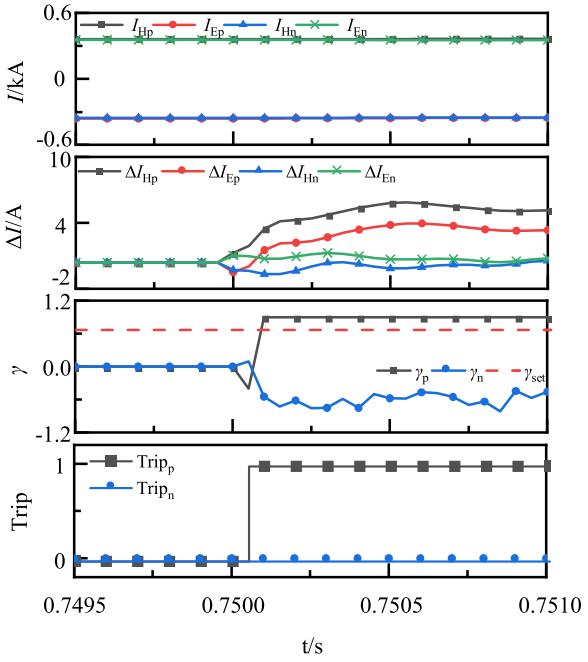

FIGURE 10. Internal PPG fault via 20Ω transition resistor under heavy load.

lines may be anomalous, at which time the protection may refuse to operate. Fig. 10 shows the protection operation in the case of a heavy load and high-resistance ground fault. Changing the total load of ports T6 and T7 from 2 MW to 4 MW, a PPG fault via 20Ω transition resistor occurs at $f2$ as an example, and the system operates until 0.75 s when a permanent fault occurs. The scheme proposed in this paper is based on the combination of fault current polarity and current GSRA judgment method, where the current under heavy load does not cause the incremental trend of the positive and negative lines on both sides of the current to change, and is unaffected by the load current.

3) THE INFLUENCE OF THE DISTRIBUTED CAPACITANCE OF THE LINE

In the traditional longitudinal protection scheme based on the change in fault current polarity, when a fault occurs, the protection may operate incorrectly because of the fluctuation

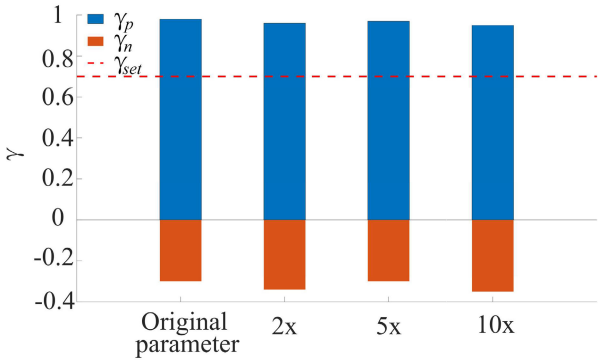

FIGURE 11. Simulation results of current correlation considering line distributed capacitance.

of the current on both sides of the line caused by the transient characteristics of the distributed capacitor. In this study, the line distributed capacitance is expanded to 2, 5, and 10 times the original value. Taking the occurrence of a PPG fault at $f2$ as an example, the simulation results of the current GSRA considering the line-distributed capacitance are shown in Fig. 11.

GSRA uses the current increments at both ends of the line for relational analysis, and the current components of the line distribution capacitance are canceled out and do not participate in the GSRA calculation process during the current increment calculation. It can be observed that when the distributed capacitance of the line increases, the fault current ratio correlation of the positive and negative lines after the fault still presents the same law as the original parameters, the protection can operate correctly, and the protection scheme is not affected by the distributed capacitance of the line.

4) THE INFLUENCE OF OPEN-LOOP OPERATION

When a fault occurs on any line and is isolated by the system, the distribution system is in an open-loop operation. While the power flowing through each port changes after an open-loop operation of the system, the incremental characteristics of the fault current do not change after a fault in any line. This paper sets 0.5 s when line L5 is out of operation with $f2$ occurring PPG fault as an example, the system operates to 0.75 s when a permanent fault occurs, and the simulation results are shown in Fig. 12.

It can be observed that the open-loop operation of the system only affects the magnitude of the fault current and does not affect the correct operation of the protection.

5) THE INFLUENCE OF CONVERTER BLOCKING AND DATA WINDOW LENGTH

A DC line generates a serious overcurrent in a short period when a fault occurs in a DC system. To prevent damage to the converter, each converter station monitors the bridge arm current in real time and sets up over-current protection. When the converter self-protection operates, the converter will be blocked, the controllable elements in the converter will be

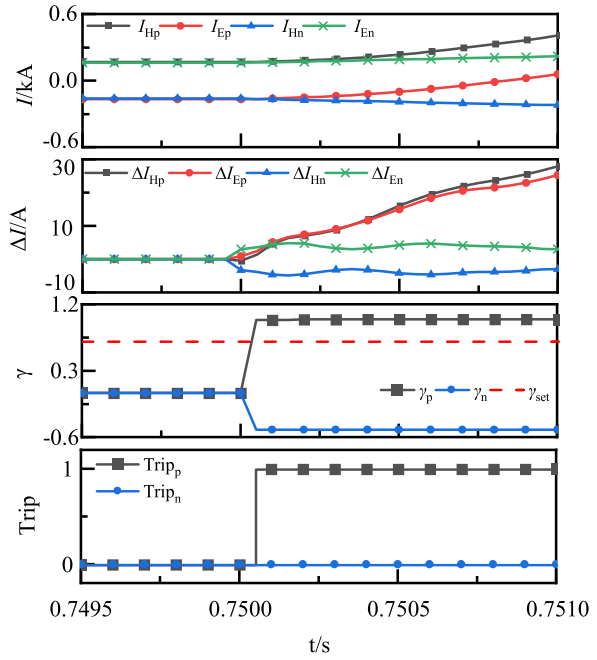

FIGURE 12. Fault simulation waveform during open-loop operation.

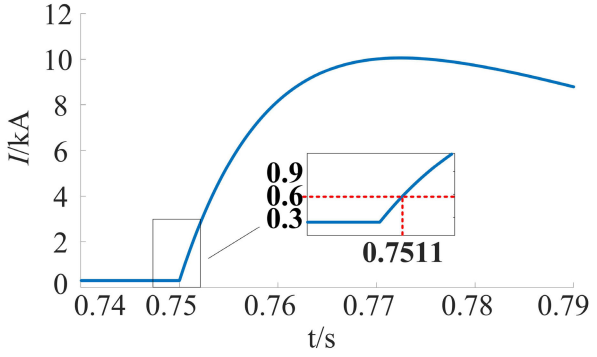

FIGURE 13. DCT bridge arm current during PP fault.

transformed into uncontrolled, and the current characteristics of the faulty line will be changed. Fig. 13 shows the bridge arm current in the DCT when a PP short-circuit fault occurs at $f2$. If the converter blocking adjustment value is 2 times the rated current, the converter will be self-protected approximately 1ms after a fault occurs.

The sampling frequency used in the simulation in this paper is 20 kHz, and the identification time of the fault after the occurrence of the fault is 150μs in total for three sampling points. Considering that the logic signal communication time required for a 5 km DC line is approximately 100μs [30], [31], the protection can be operated before the converter blocking and is unaffected by the converter. If the sampling frequency is changed to 10 kHz, nine current-ratio correlation signals can still be obtained before the converter is blocked, without affecting the protection operation.

6) THE INFLUENCE OF NOISE INTERFERENCE

The distribution system is susceptible to current transformer noise, communication channel noise and device noise. Strong

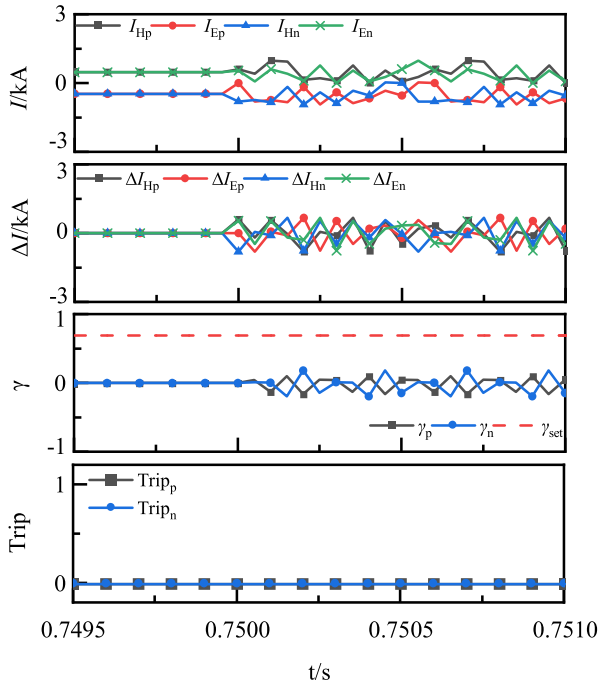

FIGURE 14. Simulation waveform under noise interference.

noise ($<$ 30 dB) may even cause changes in current increment polarity, and traditional unit protection based on current fault component polarity may be false during normal operation or rejected when a fault occurs under the action of noise [32]. Therefore, in this study, interference noise with a signal-to-noise ratio of 10 dB is added at 0.75 s during the normal operation of the system, and the simulation waveform under the noise interference is shown in Fig. 14. The interference of noise affects the current on both sides of the positive and negative lines simultaneously, which may cause the polarity and amplitude of the current to change and make the protection false. This protection scheme uses the GSRA of the positive and negative line ends of the current increments to constitute the criterion, and the fluctuation of the current has less influence on the increments. Coupled with the threshold adjustment time to consider the reliability of the scheme, the protection does not operate by mistake.

VI. CONCLUSION

This paper proposes a longitudinal protection scheme for multi-terminal flexible DC distribution lines based on fault current incremental GSRA, with comprehensive theoretical analysis and simulation verification showing that the proposed protection scheme has the following advantages:

1) The scheme considers the fault current polarity and current incremental GSRA, which are simple to calculate and meet the requirements of DC line protection speed and selectivity simultaneously.

2) The scheme does not require initiation criteria, and communication only requires transmission logic, which is

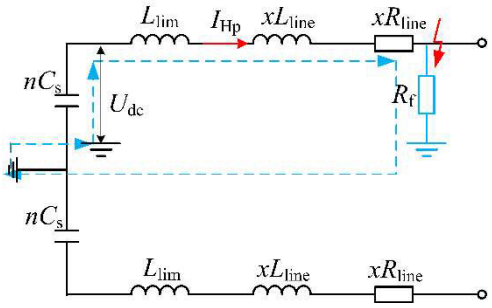

FIGURE 15. Simulation waveform under noise interference.

less demanding on system communication and has higher reliability.

3) The scheme has the ability to withstand high transition resistance and is unaffected by load current, distributed capacitance, noise interference, and converter blocking.

4) The scheme is used for a ring or radial DC grid structure and has a certain reference value for unit protection of DC lines in actual projects.

5) Double-ended volume protection relies on communication, and we will try to combine protection with artificial intelligence algorithms in future work to reduce the impact of various communication errors on protection and improve the fault tolerance of protection.

APPENDIX A

The DCT high voltage side is operated via split capacitor grounding. When a PG fault occurs in the DC line, the fault pole produces a serious overcurrent phenomenon and the healthy pole will only be slightly disturbed; when a PP fault occurs in the DC line, the bipolar line short-circuit current grows rapidly and is very likely to damage the power electronics of the flexible system. Here for more difficult to identify the PG fault than the line PP fault for the first end of the fault pole current analysis.

The length of medium voltage DC distribution system cable lines is much smaller than transmission overhead lines, and the distributed capacitance of cable lines is larger, and the transmission of traveling waves on the line will cause the distributed capacitance to charge and discharge several times. The calculation of GSRA is related to the current increment, which is mainly affected by the DC component of the current, in order to eliminate the influence of the line distributed capacitance on the measured current, the measured current at the protection installation is the filtered current after the first-order low-pass filter [32]. The filtering method is as in (9).

$$I_{\mathrm{Hp}}(j) = \tau I_{\mathrm{f}}(j) + (1-\tau) I_{\mathrm{Hp}}(j-1) \tag{9}$$

where, τ is the filtering time constant and I_f is the short-circuit current.

Therefore, the fault circuit in the capacitor discharge phase during a PPG fault can be equated to a second-order circuit as shown in Fig. 15.

In Fig. 15, C_S is the parallel capacitor of the bridge arm on the high-voltage side of the DAB, n is the number of DAB cascades, U_{dc} is the voltage to ground at the positive outlet of the inverter, I_{Hp} is the current at the positive measuring point, and R_f is not connected to the circuit in case of a metallic fault.

Combined with the above analysis, the line accounts for the proportion of the full length of x when a metallic fault occurs, that is $R_f \approx 0$, $L_{eq} = L_{lim} + xLl_{ine}$, $C_{eq} = nC_s$, $R_{eq} = xR_{line}$. The I_{Hp} expression is given in (10).

$$I_{\mathrm{Hp}} = I_0 \sin\varphi e^{-\alpha t} \sin(\omega_d t + \varphi) \tag{10}$$

where I_0 is the load current, $\alpha = R_{eq}/2L_{eq}$, $\omega_0 = 1/\sqrt{L_{\mathrm{eq}}C_{\mathrm{eq}}}$, $\varphi = \arctan\frac{2\omega_d}{R+2U_{\mathrm{dc}}/I_0}$, $\omega_d = \sqrt{\omega_0^2 - \alpha^2}$.

After a high resistance fault, the circuit is in an overdamped state and the I'_{Hp} expression is as in (11).

$$\begin{aligned} I'_{\mathrm{Hp}} = &\frac{I_0(R'_{\mathrm{eq}}C_{\mathrm{eq}} - \sqrt{\Delta}) + 2C_{\mathrm{eq}}U_{\mathrm{dc}}}{2\sqrt{\Delta}} e^{r'_1 t} \\ &- \frac{I_0(R'_{\mathrm{eq}}C_{\mathrm{eq}} + \sqrt{\Delta}) + 2C_{\mathrm{eq}}U_{\mathrm{dc}}}{2\sqrt{\Delta}} e^{r'_2 t} \end{aligned} \tag{11}$$

In (11), where $R'_{\mathrm{eq}} = R_{eq} + 2R_f$, $\Delta = {R'_{\mathrm{eq}}}^2 {C_{\mathrm{eq}}}^2 - 4L_{\mathrm{eq}}C_{\mathrm{eq}}$, and .

$$r'_{1,2} = \frac{-R'_{\mathrm{eq}}C_{\mathrm{eq}} \pm \sqrt{\Delta}}{2L_{\mathrm{eq}}C_{\mathrm{eq}}}$$

According to the measured current expression and the waveform characteristics of the fault current inside and outside the zone, it is known that the GSRA of the fault pole line is 1 when a fault occurs internal the DC line, and -1 when an external fault occurs. However, the actual engineering needs to consider noise interference, mutual sensor error, communication delay, etc. In order to avoid the maximum value of the GSRA during normal operation of the system and external faults, γ_{set} is set to 0.7.

REFERENCES

[1] D. Yang, X. Wang, W. Chen, G.-G. Yan, Z. Jin, E. Jin, and T. Zheng, "Adaptive frequency droop feedback control-based power tracking operation of a DFIG for temporary frequency regulation," *IEEE Trans. Power Syst.*, early access, May 17, 2023, doi: 10.1109/TPWRS.2023.3277009.

[2] M. E. Baran and N. R. Mahajan, "DC distribution for industrial systems: Opportunities and challenges," *IEEE Trans. Ind. Appl.*, vol. 39, no. 6, pp. 1596–1601, Dec. 2003.

[3] L. Xu and D. Chen, "Control and operation of a DC microgrid with variable generation and energy storage," *IEEE Trans. Power Del.*, vol. 26, no. 4, pp. 2513–2522, Oct. 2011.

[4] T. Hakala, T. Lähdeaho, and P. Järventausta, "Low-voltage DC distribution—Utilization potential in a large distribution network company," *IEEE Trans. Power Del.*, vol. 30, no. 4, pp. 1694–1701, Aug. 2015.

[5] S. Xue, C. Chen, Y. Jin, J. Su, T. Wei, J. He, and Y. Wang, "A research review of protection technology for DC distribution system," *CSEE*, vol. 34, no. 19, pp. 3114–3122, Jul. 2014.

[6] S. Zhang, G. Zou, X. Wei, and C. Zhang, "Bridge-type multiport fault current limiter for applications in MTdc grids," *IEEE Trans. Ind. Electron.*, vol. 69, no. 7, pp. 6960–6972, Jul. 2022.

[7] D. Kumar, F. Zare, and A. Ghosh, "DC microgrid technology: System architectures, AC grid interfaces, grounding schemes, power quality, communication networks, applications, and standardizations aspects," *IEEE Access*, vol. 5, pp. 12230–12256, 2017.

[8] L. Qi, A. Antoniazzi, and L. Raciti, "DC distribution fault analysis, protection solutions, and example implementations," *IEEE Trans. Ind. Appl.*, vol. 54, no. 4, pp. 3179–3186, Aug. 2018.
[9] L. Kong and H. Nian, "Fault detection and location method for mesh-type DC microgrid using Pearson correlation coefficient," *IEEE Trans. Power Del.*, vol. 36, no. 3, pp. 1428–1439, Jun. 2021.
[10] K. A. Saleh, A. Hooshyar, E. F. El-Saadany, and H. H. Zeineldin, "Protection of high-voltage DC grids using traveling-wave frequency characteristics," *IEEE Syst. J.*, vol. 14, no. 3, pp. 4284–4295, Sep. 2020.
[11] Z. Dai, X. Liu, Y. He, and M. Huang, "Single-terminal quantity based line protection for ring flexible DC distribution grids," *IEEE Trans. Power Del.*, vol. 35, no. 1, pp. 310–323, Feb. 2020.
[12] M. Farhadi and O. A. Mohammed, "Event-based protection scheme for a multiterminal hybrid DC power system," *IEEE Trans. Smart Grid*, vol. 6, no. 4, pp. 1658–1669, Jul. 2015.
[13] S. Yang, W. Xiang, and J. Wen, "A fault protection scheme based on the difference of current-limiting reactor voltage for overhead MMC based DC grids," *CSEE*, vol. 40, no. 4, pp. 1196–1211, Feb. 2020.
[14] S. Wenig, M. Goertz, C. Hirsching, M. Suriyah, and T. Leibfried, "On full-bridge bipolar MMC-HVDC control and protection for transient fault and interaction studies," *IEEE Trans. Power Del.*, vol. 33, no. 6, pp. 2864–2873, Dec. 2018.
[15] S. Xue, Y. Sun, B. Liu, and J. Lu, "Longitudinal travelling wave differential protection for flexible HVDC system based on Marti model," *CSEE*, vol. 39, no. 21, pp. 6288–6299, Nov. 2019.
[16] H. Zhang, W. Cong, H. Kong, M. Chen, and Z. Wei, "Longitudinal protection method for AC/DC hybrid system based on measuring current similarity," in *Proc. IEEE/IAS Ind. Commercial Power Syst. Asia (I&CPS Asia)*, Jul. 2021, pp. 1098–1103.
[17] H. Zhang, W. Cong, H. Kong, M. Chen, and Z. Wei, "Longitudinal protection method based on voltage waveform comparison for AC / DC hybrid system," in *Proc. IEEE/IAS Ind. Commercial Power Syst. Asia (I&CPS Asia)*, Jul. 2020, pp. 937–942.
[18] J. Liu, N. Tai, and C. Fan, "Transient-voltage-based protection scheme for DC line faults in the multiterminal VSC-HVDC system," *IEEE Trans. Power Del.*, vol. 32, no. 3, pp. 1483–1494, Jun. 2017.
[19] G. Song, X. Chu, X. Cai, and S. Gao, "A novel pilot protection principle for VSC-HVDC cable lines based on fault component current," *Int. J. Electr. Power Energy Syst.*, vol. 53, pp. 426–433, Dec. 2013.
[20] L. Xing, Q. Chen, Z. Gao, and Z. Fu, "A new protection principle for HVDC transmission lines based on fault component of voltage and current," *Autom. Electr. Power Syst.*, vol. 37, no. 6, pp. 1–6, Jun. 2013.
[21] S. D. A. Fletcher, P. J. Norman, K. Fong, S. J. Galloway, and G. M. Burt, "High-speed differential protection for smart DC distribution systems," *IEEE Trans. Smart Grid*, vol. 5, no. 5, pp. 2610–2617, Sep. 2014.
[22] C. Yuan, M. A. Haj-ahmed, and M. S. Illindala, "Protection strategies for medium-voltage direct-current microgrid at a remote area mine site," *IEEE Trans. Ind. Appl.*, vol. 51, no. 4, pp. 2846–2853, Jul. 2015.
[23] T. Lan, Y. Li, and X. Duan, "High fault-resistance tolerable traveling wave protection for multi-terminal VSC-HVDC," *IEEE Trans. Power Del.*, vol. 36, no. 2, pp. 943–956, Apr. 2021.
[24] S. Azizi, M. Sanaye-Pasand, M. Abedini, and A. Hasani, "A traveling-wave-based methodology for wide-area fault location in multiterminal DC systems," *IEEE Trans. Power Del.*, vol. 29, no. 6, pp. 2552–2560, Dec. 2014.
[25] M. Zakir, A. Arshad, H. A. Sher, and A. Al-Durra, "Design and implementation of a fault detection method for a PV-fed DC-microgrid with power control mechanism," *IET Electr. Power Appl.*, vol. 16, no. 9, pp. 1057–1071, Sep. 2022.
[26] M. Zakir, H. A. Sher, A. Arshad, and M. Lehtonen, "A fault detection, localization, and categorization method for PV fed DC-microgrid with power-sharing management among the nano-grids," *Int. J. Electr. Power Energy Syst.*, vol. 137, May 2022, Art. no. 107858.
[27] X. Xiao, L. Xie, and D. Huang, "Improvement and application of grey correlation degree calculation," *Statist. Manag.*, vol. 5, pp. 27–30, 1995.
[28] M. Hassan, J. Hossain, and R. Shah, "Threshold-free localized scheme for DC fault identification in multiterminal HVDC systems," *Electr. Power Syst. Res.*, vol. 210, Sep. 2022, Art. no. 108081.
[29] Z. Dai, M. Huang, H. Su, and Y. Jiao, "Single-terminal quantity based line protection for ring flexible DC distribution system," *Chin. J. Electr. Eng.*, vol. 38, no. 23, p. 12, 2018.
[30] C. Petino, M. Heidemann, D. Eichhoff, M. Stumpe, E. Spahic, and F. Schettler, "Application of multilevel full bridge converters in HVDC multiterminal systems," *IET Power Electron.*, vol. 9, no. 2, pp. 297–304, Feb. 2016.
[31] X. Wei, G. Zou, S. Zhang, and C. Xu, "Frequency domain impedance based protection for flexible DC distribution grid," *IEEE Access*, vol. 10, pp. 114203–114213, 2022.
[32] Z. Dai, Y. Li, J. Jiao, and Q. Chen, "Protection scheme for flexible DC distribution lines with high resistance and strong noise endurance ability," *High Voltage Eng.*, vol. 48, pp. 3966–3974, Sep. 2022.

ENSHU JIN received the B.Eng. and M.A. (Eng.) degrees in automation of electric power systems from Northeast Electric Power University, Jilin, China, in 1994 and 1999, respectively, and the Ph.D. degree in electrical engineering from Chonbuk National University, South Korea, in 2005. Since 2014, she has been a Professor with the School of Electrical Engineering, Northeast Electric Power University, where she is currently the Director of Teaching and Research with the Department of Relay Protection and Automation, School of Electrical Engineering. Her research interest includes power system protection and control.

XIAOCHEN HU received the B.Eng. degree in automation of electric power systems from the Shandong University of Technology, Zibo, China, in 2021. He is currently pursuing the M.A. (Eng.) degree with the School of Electrical Engineering, Northeast Electric Power University. His research interest includes protection and control of flexible DC distribution networks.

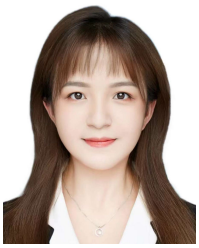

XINGRU WU received the B.Eng. degree in automation of electric power systems from Northeast Electric Power University, Jilin, China, in 2021, where she is currently pursuing the M.A. (Eng.) degree with the School of Electrical Engineering. Her research interest includes relay protection for DC power distribution systems.

SHUANGSHUANG ZHANG received the B.Eng. degree in automation of electric power systems from the Shandong University of Technology, Zibo, China, in 2022. She is currently pursuing the M.A. (Eng.) degree with the School of Electrical Engineering, Northeast Electric Power University. Her research interest includes the protection of flexible DC distribution systems.